1996 JANNAF Propulsion Systems Hazards Subcommittee Meeting, Naval Postgraduate School, Monterey, CA (4-8 Nov 96)

ANALYSIS OF THERMALLY-DEGRADING, CONFINED HMX*

M. L. Hobbs, R. G. Schmitt, and A. M. Renlund

Sandia National Laboratories, Albuquerque, New Mexico 87185†

ABSTRACT

The response of a thermally-degrading, confined HMX pellet is analyzed using a Reactive Elastic-Plastic (REP) constitutive model which is founded on the collapse and growth of internal inclusions resulting from physical and chemical processes such as forced displacement, thermal expansion, and/or decomposition. Axial stress predictions compare adequately to data. Deficiencies in the model and future directions are discussed.

INTRODUCTION

Heated energetic materials develop nonuniform porosities and high specific surface areas prior to ignition in cookoff events. Such thermal damage, created by various chemical and physical processes, enhances shock sensitivity and favors self-supported accelerated combustion. Following ignition, the subsequent level of violence depends on the competition between dynamic pressure buildup and stress release due to loss of confinement. Predictive capability within Sandia National Laboratories Engineering Sciences Center is being developed to determine the level of violence ranging from a mild pressure burst to a detonation. The present work is aimed at determining the state of the material at ignition which becomes the initial condition for subsequent dynamic analysis.

A preliminary hydrostatic stress-strain constitutive model for decomposing energetic materials under various loading conditions has been developed previously.[1] This Reactive Elastic-Plastic (REP) constitutive model is founded on the collapse and growth of internal inclusions resulting from physical and chemical processes such as forced displacement (pre-loading), thermal expansion, and/or decomposition. Stress is determined for any change in strain, temperature, and/or fraction of solid converted to gas. The REP constitutive model couples the thermal, chemical, and mechanical behavior to determine the degraded state of a reactive material. To validate and calibrate the constitutive model, Renlund et al.[2] have developed a small-scale experiment which can be used to measure the rate of pressurization of confined energetic materials subjected to a controlled thermal field.

A schematic of the hot cell experiment is shown in Fig. 1.A. The bottom and top of the hot cell experiment are cooled with chilled water to keep the load cell near ambient temperature and to prevent temperature gradients in the bolts. A radiation shield (not shown in Fig. 1) is also used to prevent temperature gradients in the bolts. A 1/4 inch diameter pellet of energetic material (EM) is confined in a cylindrical block of stainless steel (hot cell) and two opposing invar rods. O-rings are used to prevent gases from leaking out of the hot cell. An invar cage composed of two plates and six bolts, supports the load cell and the EM confinement apparatus. A thermocouple is used to measure the pellet temperature.

Figure 1.B shows a 20X magnification of PBX-9501 (95% HMX, 2.5% Estane, and 2.5% BDNPA-F) before and after a typical hot cell heating cycle. Damage is evident in the form of debonded crystals. Void formation within individual HMX crystals is not apparent until reaction threshold temperatures are reached as shown in the scanning electron micrographs (SEMs) of individual 200 μm HMX crystals in Fig. 1.C. The SEMs in Fig. 1.C were obtained from hot cell run numbers 17 and 18 which contained PBX-9501. Pellet temperature and axial force histories for run numbers 17 and 18 are shown in Fig. 1.D; a summary of both experiments, and also HMX run #26, is given in Table 1.

The force data for run #17 show a linear increase in force measured by the load cell in the first 25 minutes followed by a force relaxation from 25 minutes to 40 minutes; after 40 minutes the load increases gradually as shown in Fig. 1.D. The initial linear increase in measured force results from thermal expansion of the invar bars and the PBX-9501. The specific cause of the relaxation between 25 and 40 minutes is unknown. However, the relaxation might result from HMX solid-to-solid phase behavior combined with the viscoelastic nature of the hot rubbery binder flowing between crystals and filling defects more compactly. The phase behavior of various HMX polymorphs is discussed in more detail in the **HMX SOLID PHASE TRANSITION** section of this paper. The viscoelastic nature of the binder is beyond the scope of this paper. The force increases gradually for run #17 from 50 minutes to 200 minutes, likely due to low levels of decomposition. A scanning electron micrograph (SEM) of the PBX-9501 pellet from run #17 is shown in Fig. 1.C. Void formation was not readily evident within the 200 μm HMX crystals for run #17.

---

*Approved for public release; distribution is unlimited

†This work performed at Sandia National Laboratories supported by the U.S. Department of Energy under contract DE-ACO4-94AL85000.

A) Cross-section of hot cell

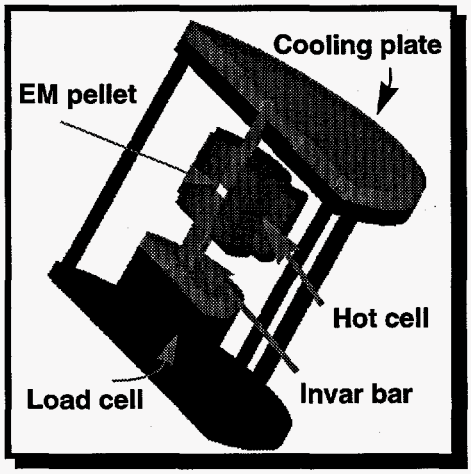

B) 20X magnification of PBX-9501

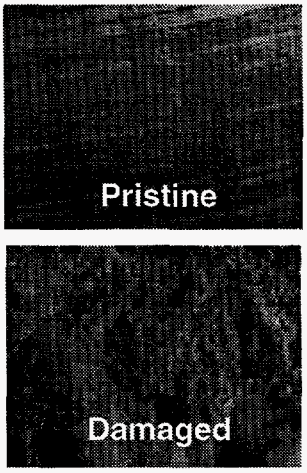

C) Scanning electron micrographs of PBX-9501 from run #17 and run #18

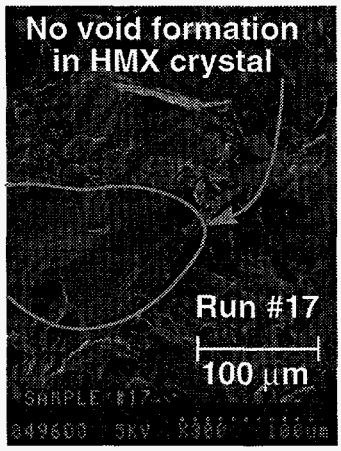

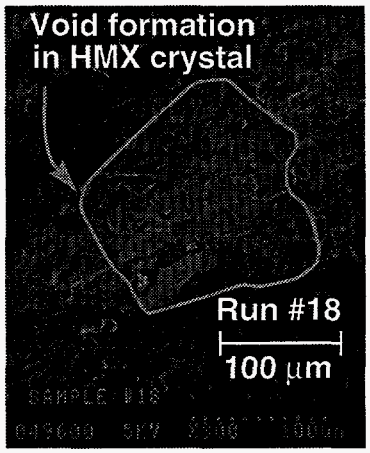

D) PBX-9501 hot cell data

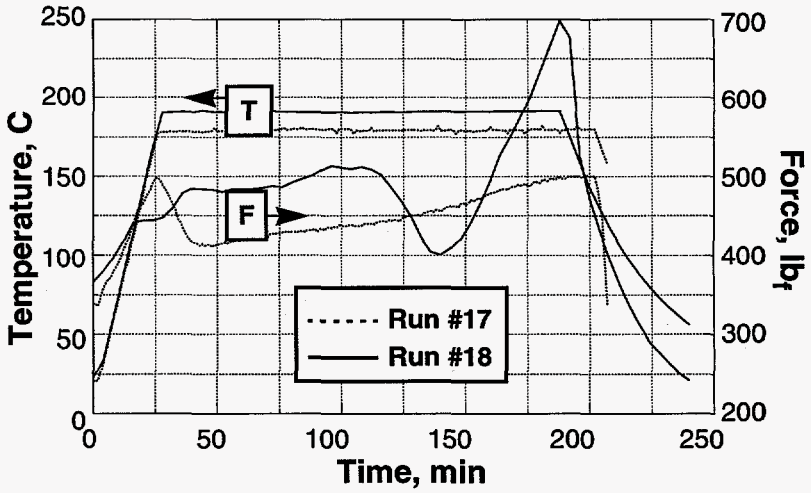

Fig. 1. A) Cross-section of hot cell showing major components, B) magnification of PBX-9501, C) scanning electron micrographs of degraded PBX-9501, and D) PBX-9501 hot cell data.

DISCLAIMER

Differences between runs #17 and #18 include pre-load and maximum pellet temperature. The higher pellet temperature (run #18) resulted in an overall 3.3% mass loss; whereas, the lower pellet temperature (run #17) resulted in 1.8% mass loss. The accuracy of the mass loss is probably within an order of magnitude given the difficulty in sample recovery. The measured force for run #18 was constant during the temperature ramp between 15 and 30 minutes; whereas, the measured force for run #17 decreased between 25 and 40 minutes. Differences between the force relaxation characteristics for these two runs during the temperature ramp might be due to the different pre-load and/or particle size distribution; however, more experiments are needed to quantify this behavior. The slight increase in load between 40 and 110 minutes for runs #17 and #18 are similar and likely due to low levels of decomposition. From 110 to 140 minutes, the measured load for run #18 decreases substantially before the onset of accelerated decomposition which causes the load to increase sharply. A scanning electron micrograph (SEM) of the PBX-9501 pellet from run #18 is shown in Fig. 1.C. Void formation is apparent within the 200 μm HMX crystals for run #18.

Table 1. Summary of selected hot cell experiments

Run #	Date	HE	Max. Pellet T, C	Initial mass, g	Initial density, g/cc	Final recovered mass, g	Final Density, g/cc	Max. force, lb_f	Vent	Mass loss,%*
17	12-14-95	9501	180	0.1832	1.8337	0.1799	1.7871	500	N	1.8
18	1-9-96	9501	191	0.1831	1.8342	0.1770	1.7499	700	N	3.3
26	4-2-96	HMX	195	0.1810	1.786	0.1516	NM†	850	Y	16

*NM - not measured

†Calculated from measured initial and final mass

SIMPLE HOT CELL MODEL

The transient hot cell model is zero dimensional in axial force and one-dimensional in temperature. An overall displacement balance forms the foundation of the model. The invar bars, load cell, and inert calibration materials are assumed to be linear elastic materials. For these elastic materials, the displacement caused by thermal expansion is treated separately. Typical values of Young's modulus, *E*, and thermal expansion coefficient, α, are used for all elastic materials except the load cell. Since the load frame is not perfectly stiff, the Young's modulus of the load cell is chosen to fit measured axial force hot cell data for a well characterized copper pellet. This calibrated material parameter was kept constant for subsequent load cell simulations. Temperature and the fraction of HMX converted to gas are assumed to be known. The REP material model,[1] assuming only hydrostatic stress-strain behavior, is used for HMX.

The overall displacement balance for the hot cell configuration shown in Fig. 2 is

$$\sum_i \delta_i = \delta_{PL} \tag{1}$$

where δ represents a displacement and *i* represents either a stress-induced displacement, temperature-induced displacement, or a displacement induced by the REP material. The displacement induced by a pre-load is represented by δ_{PL}. For the hot cell, Eq. (1) becomes

$$\delta^{\sigma}_{LC} + \delta^{T}_{LC} + \delta^{\sigma}_{IN} + \delta^{T}_{IN} + \delta_{REP} = \delta_{PL} \tag{2}$$

$$\text{where, } \delta^{\sigma}_{LC} = -\frac{\sigma l^{o}_{LC}}{E_{LC}},\ \delta^{\sigma}_{IN} = -\frac{\sigma l^{o}_{IN}}{E_{IN}} \tag{3}$$

$$\text{and, } \delta^{T}_{LC} = \alpha_{LC} l^{o}_{LC} (T_{LC}{}^{b} - T^{o}),\ \delta^{T}_{IN} = \alpha_{IN} l^{o}_{IN} (T_{IN}{}^{b} - T^{o}) \tag{4}$$

$$\text{and } \delta_{REP} = l^{o}_{REP}\, \varepsilon_{REP} \tag{5}$$

where the superscripts σ, *T*, *o*, and *b* represent stress, thermal, initial, and bulk, respectively. The subscripts *LC*, *IN*, *REP*, and *PL* represent load cell, invar bars, reactive elastic plastic material, and pre-load, respectively. The primary

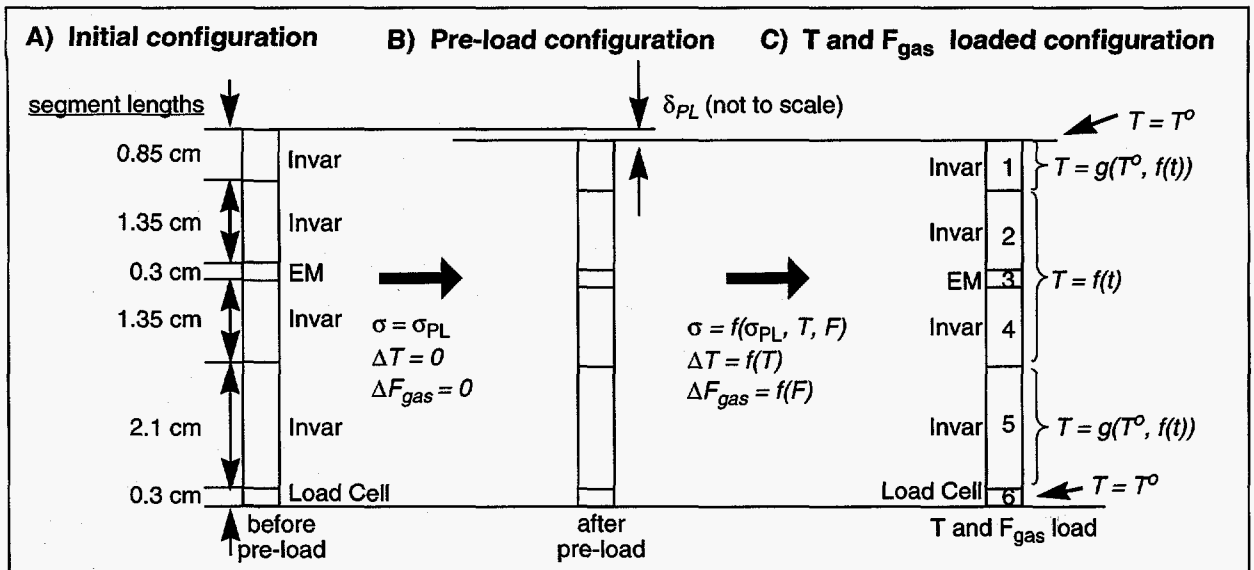

Fig. 2. Hot cell configuration used in the zero-dimensional model: A) initial configuration showing segment lengths, B) pre-loaded configuration showing pre-load displacement, δ_{PL}, and C) T and F_{gas} loaded configuration showing thermal history assumptions. The temperatures in the EM and middle section of the invar bars are assumed to be constant at any instant in time; whereas, the temperatures of the upper and lower invar segments vary linearly between T and T^o at any instant in time.

variables σ, l, E, α, T, and ε represent axial stress, length of material, Young's modulus, linear thermal expansion coefficient, temperature, and engineering strain, respectively. The pre-load displacement, δ_{PL}, is calculated to obtain a specified axial pre-load, $\sigma = \sigma_{PL}$, as discussed in the algorithm section.

For the simulations discussed in this paper, the temperature change in the load cell (section 6 in Fig. 2.C) is assumed to be zero. In other words, the load cell temperature is always assumed to be T^o. The temperature at the top of the upper invar bar (top of section 1 in Fig. 2.C) is also assumed to be equal to T^o. The temperature of the portion of the invar bar in direct contact with the hot cell (sections 2 and 4 in Fig 2.C) as well as the energetic material (section 3 in Fig. 2.C) is assumed to be spatially constant at any instant in time. This temperature is a function of time and was measured with a thermocouple in direct contact with the top of the energetic material or inert pellet. The portion of the invar bars that are not in direct contact with the hot cell (sections 1 and 5 in Fig. 2.C) are assumed to vary linearly between the measured temperature and the reference temperature, T^o. The temperature distribution is considered when calculating the bulk temperature in the invar bars.

MODEL ALGORITHM

Given the axial pre-load stress, σ_{PR}, the pre-load displacement, δ_{PL}, is calculated as follows:

$$\delta_{PR} = \delta^{\sigma,PR}{}_{LC} + \delta^{\sigma,PR}{}_{IN} + \delta^{PR}{}_{REP} \tag{6}$$

$$\delta_{PR} = -\frac{\sigma_{PR} l^o{}_{LC}}{E_{LC}} - \frac{\sigma_{PR} l^o{}_{IN}}{E_{IN}} + l^o{}_{REP}\varepsilon_{REP} \tag{7}$$

where ε_{REP} is calculated iteratively with the REP constitutive equations. Once the pre-load displacement is calculated, Eq. (2) can be solved for the stress, σ, at each load step which is determined by a change in T and/or F:

$$\sigma = (\delta_{REP} + \delta^{T}{}_{LC} + \delta^{T}{}_{IN} - \delta_{PR})/[(l^o{}_{LC}/E_{LC}) + (l^o{}_{IN}/E_{IN})] \tag{8}$$

where δ_{REP} is the displacement in the reactive material for a given change in T and/or F. The axial stress can be determined with the following algorithm:

1. Assume δ_{REP} and calculate σ with Eq. (8), $\sigma_{\Sigma\delta}$.

2. With assumed δ_{REP} calculate $\varepsilon_{REP} = \delta_{REP} / \rho_{REP}$
3. With ε_{REP} calculate σ with REP model iteratively, σ_{REP}
4. Iterate until $\sigma_{\Sigma\delta} - \sigma_{REP} = 0$.

where $\sigma_{\Sigma\delta}$ and σ_{REP} represent stress calculated by displacement balance and stress calculated with the REP material model, respectively. The solver ZEROIN[3] is used for the pre-load calculation and subsequent load step calculations.

REACTED GAS FRACTION CALCULATIONS

The simple hot cell model requires the temperature and reacted gas fraction. The reacted gas fraction is the weight fraction of HMX that is converted to gaseous products. The temperature history shown in Fig. 3.A is obtained from a thermocouple measurement which is used with COYOTE[4] or XCHEM[5] to determine the reacted gas fraction. The reacted gas fraction, calculated using the global HMX mechanism and rate constants from Tarver and McGuire,[6] is shown in Fig. 3.A. The Tarver and McGuire global HMX mechanism is described by the following reaction sequence

$$A \rightarrow B \rightarrow 2C \rightarrow D \tag{9}$$

where A, B, C, and D represent HMX, condensed intermediate, gas intermediate, and final gaseous products, respectively. The maximum predicted reacted gas fraction for HMX with the Tarver and McGuire[6] mechanism is 0.05.

The Tarver and McGuire[6] mechanism was developed to obtain proper heat release for confined thermally-degrading explosives by using one-dimensional time-to-explosion data (ODTX). The amount of HMX converted to gaseous products was not measured in the ODTX experiments. For the hot cell run #26, the BKW equation-of-state (EOS) was used to estimate the HMX reacted gas fraction using the measured force increase between 85 and 110 minutes. The average reacted gas molecular weight and BKW covolume was assumed to be 30 g/mol and 394, respectively. The volume of the gap between the invar rods and the hot cell was estimated with JAS-3D[7] using slidelines (14 μm gap) to be roughly 1% of the original pellet volume. The gap volume was calculated based on the distance from the top of the pellet to the confining O-ring, 0.1575 cm. The HMX pellet radius was assumed to be the same as the inner bore radius of the stainless steel hot cell. The height of the pellet was assumed to be the original height (0.3 cm) plus δ_{REP} calculated from Eq. (2). The gas fractions predicted with the BKW model and the Tarver and McGuire model are considerably different as shown in Fig. 3.A. The BKW prediction would be closer to the Tarver and McGuire prediction by assuming an average gas molecular weight of about 58 g/mol.

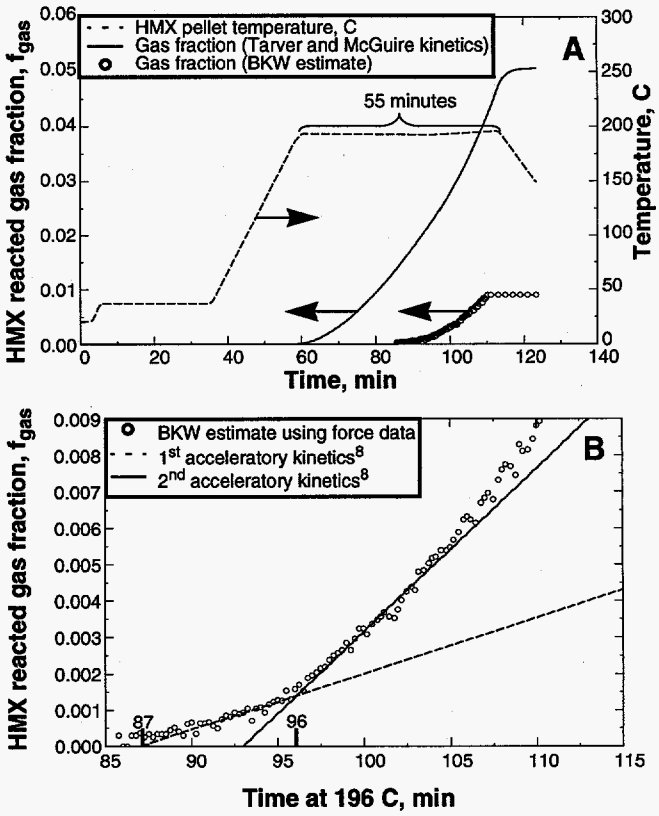

Fig. 3. HMX hot cell pellet A) temperature history and reacted gas fraction history computed using Ref. 8 kinetics. B) HMX reacted gas fraction history computed using BKW estimate and Ref 8 kinetics.

Figure 3.B shows the reacted gas fractions estimated with the BKW-EOS and an estimate using Behrens et al.[8] empirical correlation. Behrens et al.[8] studied the thermal decomposition of HMX samples (with mean particle diameters of 150 and 600 μm) between 175 and 235 C using the simultaneous thermogravimetric modulated beam mass spectrometer (STMBMS) apparatus with a focus on the initial stages of the decomposition. Weight loss data, corrected for HMX evaporation, showed 3 distinct periods: 1) induction period (little or no mass loss), 2) the first acceleratory period (slow mass loss region), and 3) the second acceleratory period (high mass loss region). The length of time for each of the three periods were shown to be temperature dependent and simple Arrhenius expressions were fit to the regions. The beginning of the induction period is the time when the sample reaches the isothermal temperature. Behrens et al.[8] noted that the end of the induction period correlated

with significant N_2O formation. No correlation was found for the end of the first acceleratory region and beginning of the second acceleratory region.

The induction time for HMX held at 196 C was calculated with the empirical correlation of Behrens et al.[8] to be 263 minutes. However, the HMX in the hot cell was held at 196 C for only 55 minutes with an induction time of approximately 25 minutes as shown in Fig. 3.A. Confined gases react exothermically and enhance solid decomposition. In a companion paper at this PSHS meeting,[9] a global model of HMX has been developed based on STMBMS data. The kinetic rate coefficients were obtained from δ-HMX decomposition data. The global HMX mechanism was successfully applied to confined cookoff tests by restricting sublimation of HMX and the mononitroso analog of HMX, and accounting for gas-phase reactions. The simulations with this global mechanism of hot cell run #26 gave similar reacted gas fraction histories as the Tarver and McGuire mechanism shown in Fig. 3.A.

Induction times for the hot cell experiment and predictions from Behrens et al.[8] empirical correlation are different. Differences in induction times are likely related to the primary differences in the two experiments: high pressure and gas confinement. Although the release rates in the first acceleratory and second acceleratory periods are similar to the BKW estimates using measured hot cell force data as shown in Fig. 3.B, the agreement is likely fortuitous. For the simulations in the present paper, the BKW estimate of reacted gas fraction is used with an induction period ending at 87 minutes, and a transition to the second acceleratory period at 96 minutes as shown in Fig. 3.B.

MODEL PARAMETERS

The primary independent variables are temperature and reacted gas fraction histories. The temperature input is provided by a direct measurement of the HMX pellet. The reacted gas fraction input, as discussed in the **REACTED GAS FRACTION CALCULATIONS** section, follows the solid and dashed line in Fig. 3.B. Other input parameters, primarily associated with the REP model are given in Table 2. A detailed discussion of the REP model parameters are discussed in Ref. 1.

A perfectly stiff experimental apparatus, with no deflection of the bottom and top plates and perfect contact at all material interfaces, should not require calibration. Since the hot cell experimental apparatus is not perfect, the load cell material was used to calibrate the model. The load cell was assumed to be an elastic material with Young's modulus adjusted to match experimental data obtained from the hot cell using a copper pellet. After the Young's modulus for the load cell was determined, this material property was assumed to be invariant. To check the calibration constant, hot cell data from aluminum and brass were reproduced using the Young's modulus calibrated with copper. The Young's modulus is denoted as eym in Table 2. Plots of the hot cell predictions and measurements for copper, brass, and aluminum are shown in Fig. 4.

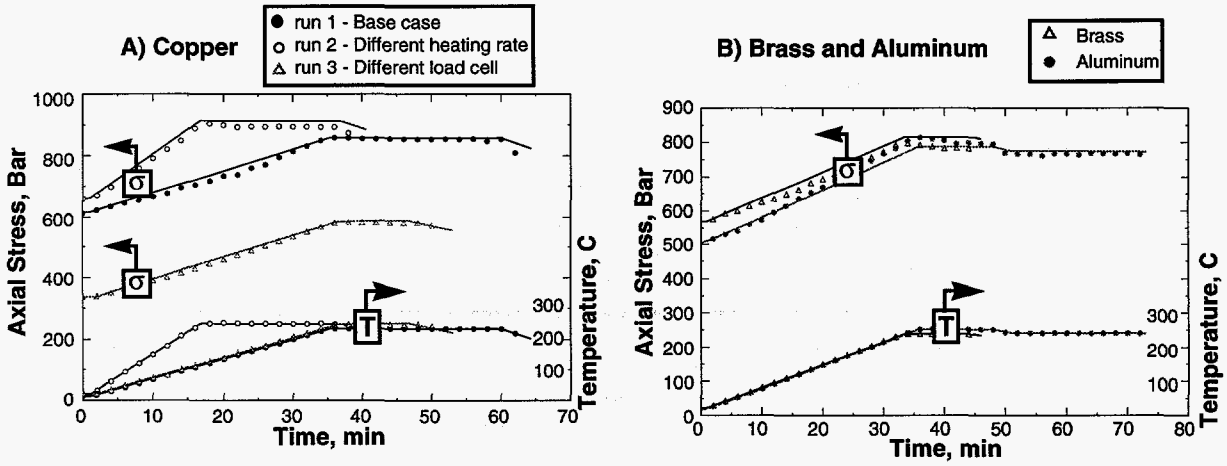

Fig. 4. Measured (symbols) and predicted (solid line) stress and temperature for A) copper, B) brass and aluminum.

MODEL PREDICTION AND COMPARISON TO EXPERIMENTAL HOT CELL DATA

Predicted and measured axial force for HMX hot cell run #26 are shown in Fig. 5.A; predicted axial and yield stresses are shown in Fig. 5.B; and, predicted gas volume fraction and pellet displacement are shown in Fig. 5.C. Between 0 and 5 minutes, the measured HMX force in Fig. 5.A increases about 30 lb_f (390 to 420 lb_f) as the sample is heated from 22 C to the preheat temperature of 28 C. The calculated force only rises by 5 lb_f during this period. The small rise in force in the calculation is attributed to elastic pore crushing as shown in Fig. 5.B and 5.C.

Table 2. Input parameters for HMX

Parameter	Value	Definition, Units
aez	1.0×10^{-12}	Absolute solver tolerance for search interval
appa	10.5	BKW parameter
beta	0.298	BKW parameter
bulkm	141,000	Bulk modulus for REP material, atm
clen	2.95	Initial length of cold invar section, cm
covol	471	BKW parameter
cv	0.24	Specific heat, cal/g-K
einv	1.44×10^{12}	Young's modulus of invar, dynes/cm^2
elc	2.38×10^{10}	Young's modulus of load cell, dynes/cm^2
expon	8.3	Exponent used in Mie-Grüneisen equation of state
gam	1.1	Mie-Grüneisen coefficient
gcon	82.06	Gas constant, cc-atm/mol-K
gmw	33.3	Molecular weight used in BKW equation of state, g/mol
hlen	2.7	Initial length of hot invar section, cm
pgas0	1.0	Reference initial pressure for gas in REP model, atm
phi0	0.055	Reference initial volume fraction for REP
phicri	0.5	Critical value of volume fraction
pr	0.3	Poisson's ration for the REP material
preld	660.8	Pre-load stress, bars
radius	0.3	Radius of rod
rez	1.0×10^{-12}	Relative solver tolerance for search interval
rhos0	1.905	Reference initial density for solid in REP model, g/cc (TMD)
rinv	5.65	Initial length of invar rod, cm
rlc	0.3	Initial length of load cell, cm
rrep	0.3	Initial length of REP material, cm
teinv	3.2×10^{-6}	Thermal expansion coefficient of invar, 1/K
telc	0	Thermal expansion coefficient of load cell, 1/K
theta	6620	BKW parameter
tmelt	520	Melting temperature used by REP, K
tref	294	Initial temperature, K
yld0	200	Yield strength, atm
yldn	0	Yield exponent
zeta	1	Modification factor for thermal expansion used by REP

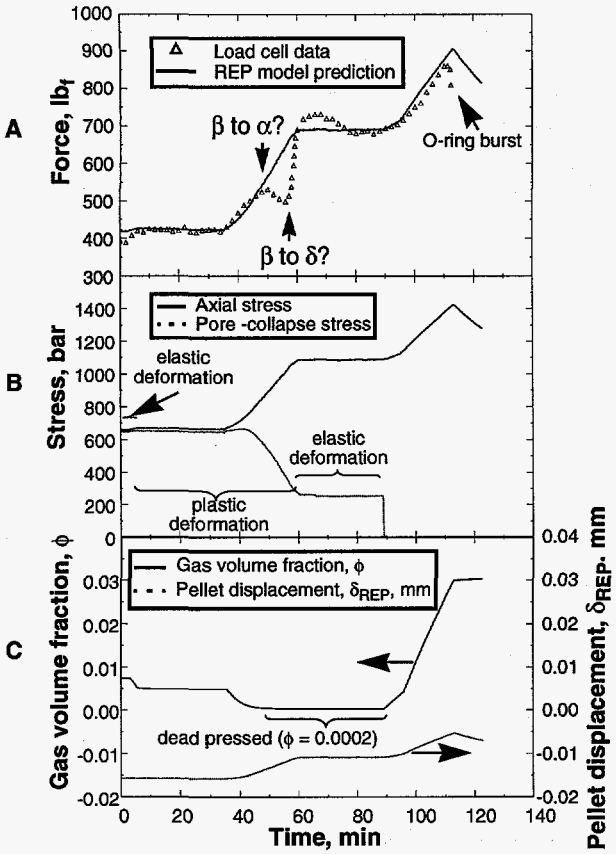

Fig. 5. HMX run #26 A) predicted and measured hot cell axial force, B) predicted axial stress and pore collapse stress, and C) predicted gas volume fraction and HMX pellet displacement. The temperature history for this experiment is shown in Fig. 3.A.

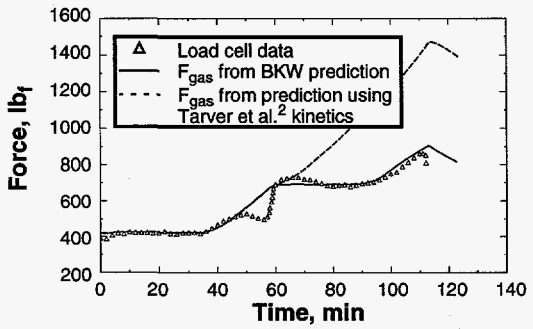

Fig. 6. HMX run #26 predicted using the reacted gas fraction predicted using the Tarver and McGuire mechanism as shown in Fig. 3.A. The data and prediction from Fig. 5. are also shown for comparison.

Between 35 and 50 minutes the measured force increases from 420 to 530 lb_f then relaxes to approximately 500 lb_f at approximately 56 minutes. The change in strain rate between 35 and 50 minutes was calculated to be nominally 10^{-5} (s^{-1}). Between 60 and 66 minutes, the force increases dramatically from 490 to 730 lb_f, likely due to the β-HMX to δ-HMX solid-to-solid phase transition. The measured force relaxes by 50 lb_f between 66 and 80 minutes. This relaxation is probably a viscoplastic effect induced by pressure and temperature dependent phase behavior as discussed in more detail in the following section. After 87 minutes significant reaction causes the force to increase rapidly.

As the pores collapse, the matrix material (condensed HMX) experiences elastic and plastic deformation as shown in Fig. 5.B. This behavior is described by the pore-collapse relations derived by Carroll and Holt.[10] As the pellet is ramped to the 190 C temperature plateau, the matrix material thermally expands which causes the pores to collapse as shown in the gas volume fraction plot in Fig. 5.C. The smaller bubble volume causes the gas pressure to increase which is in balance with the solid hydrostatic stress and the bubble collapse deviatoric stress. The HMX pellet is assumed to be dead pressed when the gas volume fraction does not decrease significantly with increasing load. For the HMX simulations in Fig. 5.B, the HMX pellet appears to be dead pressed between 50 and 90 minutes. The gas volume fraction starts to increase from the dead pressed value of 0.0002 at the onset of gas generation, near 87 minutes. Fig. 5.B shows the pellet displacement to be always negative since the pellet is being compressed.

Fig. 6 illustrates the behavior of the force prediction when the reacted gas fraction is calculated with Tarver et al.[6] kinetics as shown previously in Fig. 3.A. Differences in predicted and measured axial load may be associated with uncertainty in the solid volume related to thermal expansion, compressibility, and phase behavior of the degraded HMX.

HMX SOLID PHASE TRANSITIONS

HMX solid phase transitions, which might induce viscoplastic relaxation, were not considered in the modeling results presented in Fig. 5 or 6. The REP model only predicts force relaxation when temperature is decreased as shown from 110 to 120 minutes in Fig. 5.A. The three solid HMX phases, β-HMX (chair ring formation, 1.902 g/cc), α-HMX (boat ring formation,1.838 g/cc), and δ-HMX (boat ring formation with NO_2 functional groups on one side, 1.786 g/cc) exist.[11,12] β-HMX is the most stable at room temperature and δ-HMX is the most stable at high temperatures. As β-HMX changes to either α- or δ-HMX, the volume of the condensed phase increases. The solid volume change associated with the first phase change in run #26, noted as β to α in Fig. 5.A, is postulated to induce plastic pore crush. An increase in measured axial force due to the β to α phase change may not be apparent if the HMX pellet has sufficient porosity. The second phase change, noted as β to δ in Fig. 5.A, is postulated to cause a measurable force increase since the HMX may be dead pressed, similar to the calculation shown in Fig. 5.C.

Brill and coworkers[13-17] have measured the polymorph transition of HMX as a function of temperature, pressure and particle size and have developed a phase diagram which is shown in Fig. 7 for 63 μm HMX particles. High pressure causes δ-HMX to revert to the β-HMX. Fig. 7 also shows stress (determined by dividing the measured force by the initial cross sectional area of the pellet) plotted against three thermocouple temperatures. The actual HMX temperature for run #26 is expected to be between the thermocouple measurements. Brill's data indicate that a phase transition should not have occurred in run #26 due to the high pre-load, yet the load cell force measurements shows phase change behavior. Perhaps the α-δ phase diagram is more appropriate for the hot cell. Gibbs and Popolato[12] report the α to δ atmospheric phase change to occur at 160 C. Also, larger particles with confined decomposition gases may explain differences between the hot cell HMX phase behavior and Brill's data. Karpowicz and Brill[16] attribute the particle size effect to high pressure produced by greater buildup of decomposition products within the crystals of larger particles. Gaseous products trapped within the lattice may create higher stresses within the material and thus maintain the HMX in the beta phase at lower applied pressures. In the HMX hot cell experiment, a large particle size distribution as well as dramatic stress increases may lead to nonintuitive force histories, such as stair-step behavior, during phase transitions.

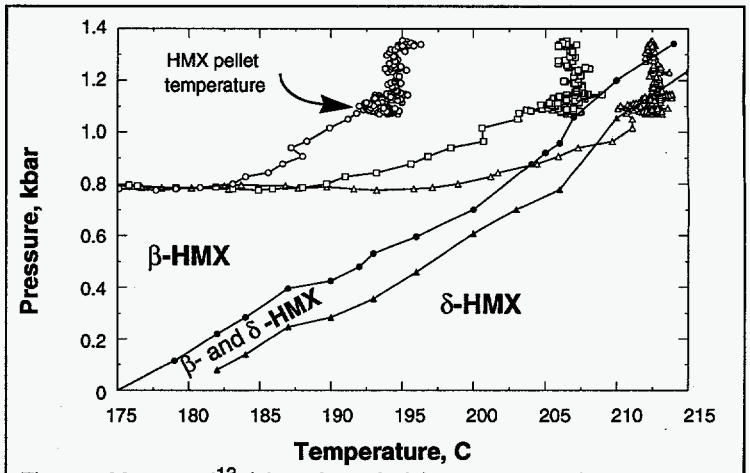

Fig. 7. Measured[13] (closed symbols) pressure and temperature dependent phase behavior of β- and δ-HMX showing a region with both phases present. Open symbols represent the hot cell HMX axial stress plotted against thermocouple measurements. The open circles, squares, and triangles are for thermocouples located near the HMX pellet, in the hot cell away from the heater clamps, and in the hot cell near the heater clamps, respectively.

The cause of the force relaxation following the two apparent phase changes in the HMX hot cell data is unknown. As the pressure increases, formation of β-HMX from α- or δ-HMX, as implied in Fig. 7, might cause the measured force to decrease. Also, dramatic changes in crystalline morphology during phase transformations are expected to cause slippage and better compaction. Such viscoplastic behavior is also expected to cause relaxation. More experimental data is necessary to model the specific cause of this viscoplastic behavior.

SUMMARY AND CONCLUSIONS

A simple model of the hot cell experiment utilizing the Reactive Elastic Plastic constitutive model (REP) discussed previously[1] has been described and applied to copper, brass, aluminum, and HMX. The data show an increase in axial force, due to thermal expansion, gas formation, and phase change; as well as a decrease in axial force (relaxation) possibly due to phase change induced viscoplastic behavior. The REP model has been shown to provide adequate predictions of thermal expansion and gas induced pressurization. However, the present form of the REP model does not predict force relaxation unless the temperature or reacted gas fraction is decreased. Future versions of the REP model should account for phase change and other relaxation mechanisms. More experimental data taken at similar conditions of the hot cell (1,000-2,000 atm) under confinement are needed to develop such models.

The primary independent REP variables are temperature and reacted gas fraction histories. The temperature input was provided by a thermocouple measurement, and the reacted gas fraction was predicted by COYOTE using the Tarver and McGuire[6] kinetic mechanism for HMX. The reacted gas fractions, predicted with Tarver and McGuire kinetics, were not consistent with simple BKW estimates of the reacted gas fractions using the measured force data. However, the gas formation rates were in agreement with the simple mechanism deduced from STMBMS data by Behrens et al.[8]; although, the induction time and transition between the two acceleratory periods were different. Behrens et al.[8] HMX correlation predicted a 263 minute induction period whereas the data indicated an induction period of approximately 30 minutes. Also, the first acceleratory kinetic regime accounted for reaction of only $1/10^{th}$ of 1 percent of the HMX before the second acceleratory regime began.

Differences between the hot cell experiment and STMBMS experiment include pressure (1500 atm vs 1 atm), gas confinement (high vs low), and reaction detection methods. The hot cell experiment measures gas formation directly as an increase in axial force. The STMBMS experiment detects gas generation after formation, bubble nucle-

ation and growth, bubble failure, crack growth, and gas transport. A single mechanism which predicts the extent of reaction, particularly the amount of gas formation, in both experiments is needed. Such a mechanism should be applicable between atmospheric pressure and high pressure with the gases either being allowed to escape or remain within the confinement. More details on HMX decomposition are presented in a companion paper.[9]

The current work has discussed several advances in understanding thermally decomposing HMX under confinement. These advances come from both experimental observation and analysis of data. Additional experiments and improved modeling are necessary to advance our understanding of decomposition during cookoff. The effect of particle size distribution, measurement of the reacted gas fraction, and high pressure phase behavior should be investigated experimentally. Damage, phase change, chemical stress relaxation, viscoelastic, and viscoplastic response should be investigated further including deviatoric behavior with the coupled COYOTE/JAS code.

ACKNOWLEDGMENT

We wish to express our appreciation to Mel Baer, Rich Behrens, Ken Erickson, Sandra Klassen, Art Ratzel, and Gerry Wellman at Sandia National Laboratories for critically reviewing this paper.

REFERENCES

1. Hobbs, M. L., Baer, M. R., and Gross, R. J., "A Constitutive Mechanical Model for Energetic Materials," *Twentieth International Pyrotechnics Seminar*, IIT Research Institute, Colorado Springs, Colorado, 423 (1994).
2. Renlund, A., Miller, J. C., Hobbs, M. L., and Baer, M. R., "Experimental and Analytical Characterization of Thermally Degraded Energetic Materials," *JANNAF Propulsion Systems Hazards Subcommittee (PSHS) Meeting*, NASA Marshall Space Flight Center, Huntsville, AL (1995).
3. Shampine, L. F. and Watts, H. A., "ZEROIN, A Root-solving Code," Sc-tm-70-631, (1970).
4. Gartling, D. K., and Hogan, R. E., "Coyote II - A Finite Element Computer Program for Nonlinear Heat Conduction Problems Part II - User's Manual," SAND94-1179. IC-905, Sandia National Laboratories, Albuquerque, NM (1994).
5. Hobbs, M. L., Baer, M. R., and Gross, R. J., "Modeling Ignition Chemistry," *JANNAF Propulsion Systems Hazards Meeting*, Fort Lewis, WA (1993). See also Gross, R. J., Baer, M. R., and Hobbs, M. L., *XCHEM-1D A Heat Transfer/Chemical Kinetics Computer Program for Multilayered Reactive Materials*, SAND93-1603, UC-741, Sandia National Laboratories, Albuquerque, NM (1993).
6. McGuire, R. R. and Tarver, C. M., "Chemical Decomposition Models for the Thermal Explosion of Confined HMX, TATB, RDX, and TNT Explosives," *Seventh Symposium (International) on Detonation*, NSWC MP 82-334, Annapolis, Maryland, 56 (1981).
7. Blanford, M., "Release 1.2 of JAS3D," internal memo to distribution (March 26, 1996).
8. Behrens, R. and Bulusu, S., "Thermal decomposition of HMX: Low Temperature Reaction Kinetics and their use for assessing Response in Abnormal thermal Environments and Implications for Long-Term Aging," *Ma. Res. Soc. Symp. Proc.*, **418**, Materials Research Society, 119 (1996). See also Minier, L., Behrens, R., and Bulusu, S., "Comparison of the Thermal Decompositions of HMX and 2,4-DNI for Evaluation of Slow Cookoff Response and Long-Term Stability," *JANNAF Propulsion Systems Hazards Subcommittee (PSHS) Meeting*, NASA Marshall Space Flight Center, Huntsville, AL (1995).
9. Hobbs, M. L. "A Global HMX Decomposition Model," *1996 JANNAF Propulsion Systems Hazards Subcommittee Meeting*, Naval Postgraduate School, Monterey, CA (1996).
10. Carroll, M. M. and Holt, A. C., "Static and Dynamic Pore-Collapse Relations for Ductile Porous Materials," *J. Appl. Phys.*, 43 (4), 1626 (1972).
11. Brill, T. B., and Reese, C. O. "Analysis of Intra- and Intermolecular Interactions Relating to the Thermophysical Behavior of α-, β-, and δ-Octahydro-1,3,5,7-tetranitro-1,3,7-tetrazocine," *J. Phys. Chem.* **84**, 1376 (1980).
12. Gibbs, T. R., and Popolato, A., *LASL Explosive Property Data*, University of California Press, Berkeley, CA, 45-46 (1980).
13. Landers, A. G., and Brill, T. B., "Pressure-Temperature Dependence of the β-δ Polymorph Interconversion in Octahydro-1,3,5,7-tetranitro-1,3,5,7-tetrazocine," *J. Phys. Chem.*, **84**, 3573 (1980).
14. Goetz, F., Brill, R. B., and Ferraro, J. R., "Pressure Dependence of the Raman and Infrared Spectra of α-, β-, γ-, and δ-Octahydro-1,3,5,7-tetranitro-1,3,5,7-tetrazocine," *J. Phys. Chem.*, **82** (17), 1912 (1978).
15. Goetz, F. and Brill, T. B., "Laser Raman Spectra of α-, β-, γ-, and δ-Octahydro-1,3,5,7-tetranitro-1,3,5,7-tetrazocine and Their Temperature Dependence," *J. Phys. Chem.*, **83** (3), 340 (1979).
16. Karpowicz, R. J. and Brill, T. B., "The β → δ Transformation of HMX: Its Thermal Analysis and Relationship to Propellants," *AIAA Journal*, **20** (11), 1586, (1982).
17. Brill, T. B., and Karpowicz, R. J., "Solid Phase Transition Kinetics. The Role of Intermolecular Forces in the Condensed-Phase Decomposition of HMX," *J. Phys. Chem*, **86**, 4260 (1982).